Energy & Buildings 237 (2021) 110817

Contents lists available at ScienceDirect

Energy & Buildings

journal homepage: www.elsevier.com/locate/enb

Evaluation of changes in surface temperature of TiO_2 functionalized pavements at outdoor conditions

Maria Fernández-Mira, Eva Jimenez-Relinque, Isabel Martínez, Marta Castellote *

Eduardo Torroja Institute, Spanish National Research Council (IETcc-CSIC), Serrano Galvache 4, Madrid 28033, Spain

ARTICLE INFO

Article history:
Received 1 October 2020
Revised 18 December 2020
Accepted 4 February 2021
Available online 11 February 2021

Keywords:
TiO_2 photocatalytic pavement
Outdoor
Surface temperature
Reflective
Colour
Roughness
Urban heat island

ABSTRACT

Surface temperature of ten different materials (combination of different commercial TiO_2-based photocatalysis on different types of substrate) located outdoors have been recorded for a 12-hours period using an infrared thermography camera after 2 years of exposure to environmental conditions. Twin conventional pavement's substrates (asphalt, and three kinds of tiles) were also evaluated as a reference. A detailed optical, chromatic, and textural characterisation was performed and statistical analysis was carried out to further understand the significance of the parameters that control the surface temperature changes. It generally seems that the mean daily surface temperature and temperature range of the TiO_2 modified materials are lower than their corresponding conventional material. The observed differences on the thermal behavior does not seem to be directly related to the TiO_2 photocatalytic effectiveness. The emissivity values do not show significant variations by the application of the nano-TiO_2 additives. A multivariable correlation has allowed to deduce that main contribution to the lower temperature in the photocatalytic pavements is due to the smoother surface induced by the addition of the photocatalyst.

1. Introduction

The climate effect called Urban-Heat-Island (UHI) is a phenomenon where the air temperature in urban areas becomes several degrees higher than in its rural surroundings. The main causes of the UHI effect is the substitution of natural vegetation with the urban fabric, conformed mainly by paved roads, concrete surfaces, asphalt, roof tops, and building walls. These built surfaces are characterised by high solar absorption, very low permeability and thermal properties that enhance the energy storage and the heat release [1].

Roof and building façades of construction structures are significant contributors to the UHI [1,2]. The exterior surface temperature increases and is later transmitted inside, causing thermal discomfort, and precipitating greater cooling energy consumption [3]. For more than 100.000 population cities, the energy consumption increases by up to 2% for each degree higher in the city's air temperature [4] and the HVAC (Heating, Ventilation and Air Conditioning) consumption increases between 20% and 100% [5–9]. This raise in the demand for energy also causes an increase in atmospheric pollution, and therefore human health problems in two different ways: directly, when the higher temperatures trigger atmospheric flue gas reactions, producing the so–called SMOG (a blend of smoke and fog); and indirectly with the release of pollution gases by energy generation plants [4,10].

Pavement surfaces also play a determinant role on the overall urban thermal balance because they cover quite a high percentage of the urban fabric [1,11]. For various USA cities it was found to cover a range between 29% and 45% [12,13]. Paved surfaces in Europe and USA, consist mainly of concrete and asphalt surfaces that present high surface temperatures during the summer period [13]. Especially, the thermal properties of asphalt and their albedo (4% for black asphalt shingles and 5–10% for dark coloured conventional asphalt shingles using a two-layer process [14]) are quite significant determinant factors in their contribution to the UHI effect, reaching upwards of 60 °C on hot summer days [15].

The use of 'cool materialś is considered to be one promising and powerful technique to mitigate the UHI phenomenon Cool pavements can be classified into several types: reflective cool pavements, evaporative cool pavements, and heat storage pavements [11,16]; among them, reflective pavements are the most commonly used material due to its better thermal behaviour results [11]. Reflective pavements are characterized by high solar reflectance/albedo and high infrared emittance thus it helps to contribute to decrease the surface temperature and the sensible heat release [11,14,16].

* Corresponding author.
E-mail address: martaca@ietcc.csic.es (M. Castellote).

https://doi.org/10.1016/j.enbuild.2021.110817
0378-7788/

From laboratory testing to large scale applications, reflective pavements have demonstrated their potential to reduce the surface temperature and improve thermal conditions in urban areas. Synnefa et al. [17] reported the measured solar spectral properties and the thermal performance of 10 prototype cool coloured coatings on concrete tiles. The results evidenced a lower surface temperatures for all the cool coloured coatings. Doulos et al.[18] studied the impact of color, surface roughness and sizing on the thermal performance of 93 commonly used pavement materials outdoors during the summer period. The collected data have been extensively analysed using statistical techniques and classified according to their thermal performance and physical properties into 'cool' and 'warm' materials. Therefore "cold" materials are those having a smooth and light colored surface and construction materials made of marble, mosaic and stone. Similarly "warm" materials could be defined as those having a rough and dark colored surface and construction materials made of pebble, pavestone and asphalt. Santamouris et al. [19] and Kyriakodis et al. [20] studied the thermal impact of a large applications of reflective pavements in urban parks (4500 m^2 of light-yellow concrete tiles) and a combination of light-yellow asphalt and white concrete (37000 m^2 total zone) respectively. It was demonstrated that the use of cool paving materials contributes to the reduction of the peak ambient temperature during a typical summer day and the surface temperature in the tested parks was decreased.

Conventional titanium dioxide (TiO_2), mainly micro-sized rutile crystal form, is the most widely used white reflective pigment for the development of cool materials. Its advantages include a high refractive index, strong covering power, and good thermal performance [21,22]. Nanosized TiO_2 is growing on demand due to enhanced absorption of UV light [21] and the associated environmental benefits that include the ability of removing a broad range of organic and inorganic pollutants from air through photocatalytic redox reactions. Beside this, their self-cleaning properties contribute to maintain the initially high albedo values over the time [23]. Due to multifunctional properties, nano-TiO_2 additive is already in use on urban construction structures, façades and pavements [24–29]. However, little literature reports the effect of nano-TiO_2 application in building materials on cooling property. Some studies investigated the influence of optical properties and lightness on the thermal performance of TiO_2 coatings [11,30]. Song et al. [22] studied the effect of particle size distribution on the optical properties of titanium dioxide rutile pigments and their applications in cool non-white coatings. The results evidenced that the solar and VIS reflectances, as well as the lightness of the coatings and films pigmented with titanium dioxide pigments, decrease as the particle size of the pigments increases, while their NIR reflectance and VIS transmittance increase as the particle size of the pigments increases. Also, there are some studies focusing on the application and development of different nano-TiO_2 funcionalized construction materials. Carnielo et al [1] evaluated the thermal behavior in laboratory and under real conditions of TiO_2 based photocatalytic cement mixture with various pigments colour onto asphalt substrate. The study demonstrated that the maximum temperature differences between green, blue and grey samples respect to the original asphalt ranged between 8 and 10 °C. Lower values were obtained for the red asphalt, while the difference got close to 20 °C for the off-white samples. Zheng et al. demonstrated that the functionally with self-developed nano-reflective coating of asphalt reduced the temperature of the pavement itself and the atmosphere surface layer near the pavement. The convective heat decreased nearly 50% when compared with the control asphalt pavement. Qi et al. [31] demonstrated that the addition of rutile nano-TiO_2 in a poly acrylonitrile-styrene-acrylate resin, at a weight concentration of 5%, resulting in a better NIR and solar reflectance, high thermal emissivity, and thus excellent cooling capability.

These studies have confirmed the potentialities of nano-TiO_2 as reflective and cool materials. However, a comprehensive analysis of the effect of different types of photocatalysts applications on different substrates after been exposed outdoors, weighting the different aspects involved in the temperature finally reached at the surface has not been undertaken. To tackle these issues, in this work, different TiO_2 configurations (emulsions sprayed, slurry admixtures; and built-in) on two different substrates (asphalt and tiles) were implemented at platform scale. The platform was set up under outdoor exposure conditions at the Institute of Science of Construction Eduardo Torroja in Madrid, Spain. The surface temperature on 12 h basis of the total number of 10 types of TiO_2 nano-functionalized pavement materials combinations were measured and compared to their respective conventional materials. The temperature measurements were obtained through infrared (IR) thermograph imaging. The collected data have been analyzed statistically in order to identify the impact of TiO_2 functionalization (based on the NOx gas removal efficiency by photocatalysis) on the thermal balance of these materials. The impact of spectral reflectance, color, surface roughness have been analyzed as well. It is important to outline that this work has to be considered as a part of a whole life-cost cycle analysis of the whole implementation, to have a complete picture of the sustainability of this kind of solutions.

2. Experimental

2.1. Materials

Ten materials were analysed. "Material" refers here to the combination of a specific patented/commercial TiO_2-based photocatalytic product applied to a certain type of conventional substrate, distinguished into asphalt (24.6% of air voids as determined according to UNE-EN 12697-08:2008) or three different paving tiles. The materials resulted in three emulsions sprayed onto the surface of asphalt and paving tiles; two cementitious slurry admixtures applied to asphalt; and factory-supplied tiles with TiO_2 built-in. The materials types that will be used from now on were labelled as shown in Fig. 1. The compositional characteristics of the materials, been commercial, cannot be disclosed for reasons of industrial confidentiality. For comparison purposes, the 4 substrates without the photocatalytic product (asphalt (A) and three different tiles (T1-T3)) were also implemented

2.2. Slabs implementation and description of the experimental site

The materials and substrates without TiO_2 were placed on especially designed platform of slabs, as the pilot-scale experimental

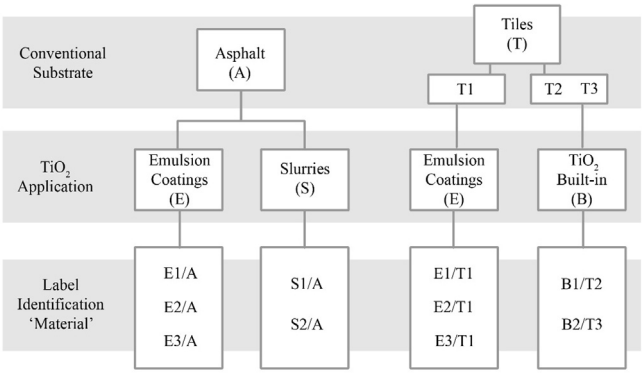

Fig. 1. Material's types and labels.

site of LIFE-Photoscaling project. They were cast between October and November 2016 and each slab measured at least 1 m^2. Prior to the construction of the platform slabs, it was necessary to prepare the ground. First of all, mechanical levelling of the working area was carried out, and a concrete slab of around 900 m^2 with a height of 20 cm was constructed to guarantee that all the materials were put on the same base. The platform slabs were kept outdoor at the premises of the Institute of Science of Construction Eduardo Torroja in Madrid city (Spain), The platform were equipped with a meteorological station that registered the relative air humidity, air temperature, sun irradiation, rainfall intensity, wind velocity and direction (Fig. 2). More details on the construction and description of the platforms can be found in [32,33].

2.3. Laboratory tests

2.3.1. Photocatalytic activity: nitrogen oxide (NOx) removal test

The initial photocatalytic activity of the materials was estimated based on the ISO standard 22197-1:2007. The freshly prepared samples with the corresponding photocatalytic materials were placed in a flow-type reactor where model air containing 1000 ± 50 ppb NO, at 25 ± 2.5 °C and humidity 50 ± 5%, was supplied through a flow-controlling system with a rate 3 ± 0.15 L/mi n. In the present work, the test gas was allowed to flow into reactor without irradiation for 30 min. After 30 min, the gas flow as maintained and the sample was irradiated during 30 min at 10 W/m^2. After this period, the light turns off under the same flow conditions for a further 30 min. The NOx (NO + NO_2) concentration of the gas was monitored using a chemiluminescence analyzer (AC-32 M, Environment S.A.). Using the data of NOx recorded during the irradiation, the amount of NO removed and NO_2 formed by the test sample was calculated by applying integration over the areas enclosed between the curves of the monitored gas concentration and the horizontal lines for the initial gas concentration taken on the time interval corresponding to the illumination period. Detailed description of the experimental set up and calculations can be found in [34,35].

2.3.2. Reflectance and colour measurements

Reflectance measurements were carried out on every specimen with the spectrophotometer Shimadzu UV-2600 equipped with a diffuse reflectance accessory sphere. The chromatic characterization was conducted using a portable sphere type spectrophotometer (CM-2300d Konica Minolta). Measurements were carried out also on the specimens (5 times on each material) under the following conditions: colour coordinates L*a*b* space, D65 illuminant (daylight with ultraviolet radiation) at 10° viewing angle and wavelength range between 360 nm and 740 nm. From these coordinate values, the whiteness index (WI) (distance from a 'perfect' white, i.e. L = 100, a = 0, b = 0)) was calculated by:

$$WI = \sqrt{(100 - L^*)^2 + (a)^2 + (b)^2} \quad (1)$$

where a WI = 0 means a pure white (100, 0, 0) surface and a WI = 100 means a pure black (0, 0, 0) surface.

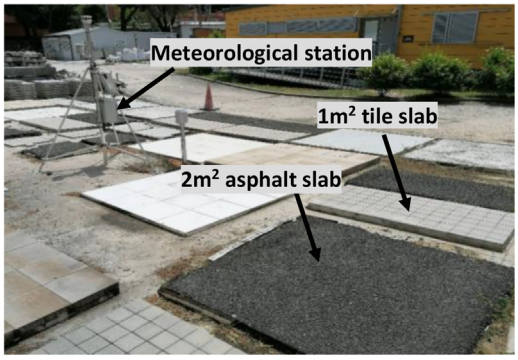

Fig. 2. Site of the experimental testing with the slabs of the different materials.

2.3.3. Surface texture

Digital images processing of cross-section of analysed specimens was used to assess the surface roughness by Image J program (roughness plugin). Previous work demonstrated the suitability of this practical approach for surface structural parameters quantification [36,37]. The measuring procedure could be summarized as follows: i) Capturing a RGB image of the work piece ii) Convert the captured image into gray scale image with the range of 0 to 255 scales. iii) Calculate the pixel distance between two adjacent deep scratches. The luminance of an image is interpreted as height for the plot. Internally the image is scaled to a square image using nearest neighbour sampling. Gaussian filtering is used to separate the waviness from the roughness and thus assess the structure at different wavelengths. The results are a 3D topographic profiles, and contains different roughness parameters. In this study the roughness parameter, Ra (arithmetical mean deviation), was selected for sample comparison.

2.4. Thermographic evaluation on pilot scale in outdoor exposure conditions

The experimental equipment used for the surface temperature measurements of all materials consists of an infrared thermographic camera FLIR B335 with a spectral range of 7.5 μm to 13 μm and an NETD thermal sensitivity of 50mK. The surface temperature image measurements were taken on an hourly basis from 8:00 to 20:00 of February 19th, 2020. Using the area measurement of the thermographic software tool (FlirTools), maximum, minimum, and average temperatures of the desired surface area were obtained.

Non-contact infrared technology provides apparent surface temperatures data, since the camera receives the total radiation coming from the object (sum of emitted and reflected radiation), so certain material and climatic parameters are necessary to compensate those apparent temperatures and perform a correct thermal comparison between the different platforms. In addition to the working distance (1 m) and the air temperature (T_{air}) and relative humidity (data included in Fig. 3), the reflected apparent temperature (T_{refl}) and the emissivity (ε) are needed. Reflected apparent temperature (T_{refl}) is the apparent temperature of other objects that are reflected by the target into the infrared camera [38] and were obtained following the ISO 18434-1:2008(E) reflector method.

Specimens samples were evaluated on laboratory control conditions. An infrared reflector (a crumpled and re-flattened piece of aluminum foil) was placed in the same plane as the target surface. Then, the apparent surface temperature of the reflector was measured with the camera. This noted temperature is the apparent reflected temperature of the measured object. The emissivity (ε) represents the ratio of a target surface's radiance to that of a black body at the same temperature and over the same wavelength in the spectral interval. Values between 0 and 1 [38]. Emissivity (ε) was calculated using two different procedures. The first one is obtained via infrared thermography technology following the ISO 18434-1:2008c (E) standard. A specific emissivimeter was also used. The average of both measurements was used as the corrective parameter on the thermographic pictures.

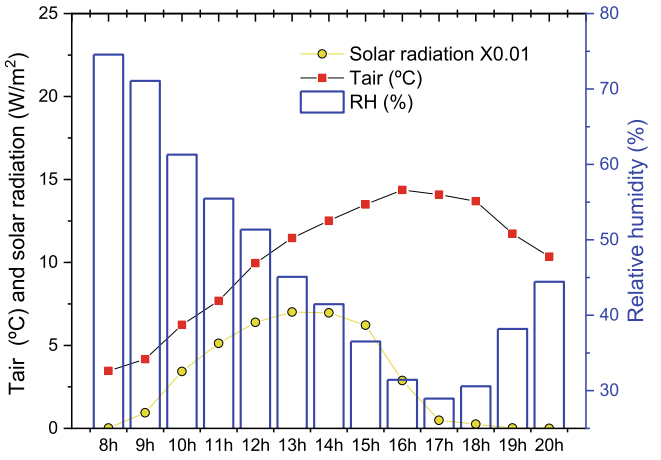

Fig. 3. Mean hourly 12-hour distribution of ambient temperature (Tair), relativity humidity and solar irradiation (×0.01).

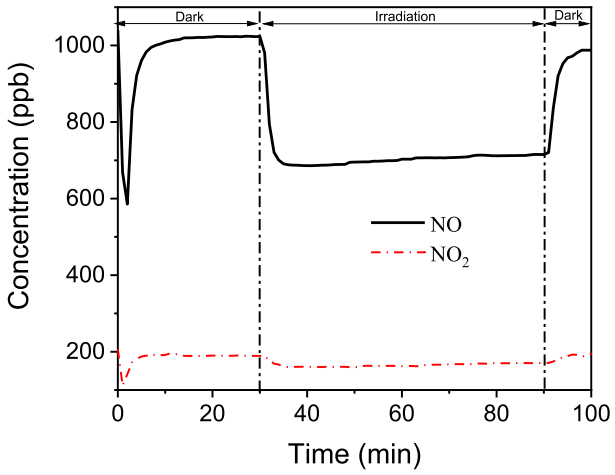

Fig. 4. Time-dependent concentration profile for NO and NO_2 of S1/A sample.

3. Results and discussion

The climatological data, from a meteorological station placed next to the platforms are given in Fig. 3. They are characterized by a highest radiation peak at 1 p.m., whereas higher air temperature took place at 4 p.m. Relative humidity decreases from its highest value at 8 a.m. (74.55%) down to 29.99% at 5 p.m., and then go up again to 44.44% at 8 p.m. Wind speed was always low during the experimental period (<1.2 m/s). Thus, the effect of wind speed on the temperature of the materials was almost negligible.

3.1. Photocatalytic performance: NOx removal efficiency

The percentage of NOx degradation (RNOx) of the selected materials based on the standard laboratory test (ISO 22197-1:2007) at initial time were included in Table 1. The NOx removal efficiency resulted in the following ranking: E3/T1 > S1/A > B2/T3 > E2/T1 > E3/A > E1/T1 > S2/A > E2/A > B1/T2 > E1/A. Fig. 4 include an example of the typical time-dependent concentration profile for NO and NO_2 during gas-phase photocatalytic NO oxidation activity tests.

3.2. Reflectance and chromatic characterization

Fig. 5 presents the spectral reflectance of conventional and TiO_2 modified samples. From these data, the integrated area in the relevant spectra ranges (UV, visible, near infrared and total solar range) were included in Table 2. The chromatic CIELAB coordinates and the whiteness index calculation of materials were also given in this table.

Table 1
Removal of NOx (%) of materials (ISO 22197-1:2007).

Material	RNOx (%)
S1/A	26.91
S2/A	7.20
E1/A	0.18
E2/A	6.40
E3/A	13.60
E1/T1	10.84
E2/T1	19.00
E3/T1	25.70
B1/T2	4.60
B2/T3	22.90

A (conventional asphalt) presents the lowest reflectance, between 0.025 and 0.055 a.u., throughout the whole wavelength range. S2/A, E2/A and E3/A also present low reflectance, with a light increment from 350 nm (0.08–0.15 a.u.). S1/A suffers a high reflectance increment also from 350 nm wavelength reaching up to 0.61 a.u.. T1 (conventional paving tile) presents 0.12 a.u. reflectance between 200 and 280 nm, and then reaches up to 0.4 a.u. at 600 nm, maintaining approximately this value until the end of the measurement wavelength range. In none of these cases, an increment of UV absorbance due to the TiO_2 addition is observed. Both emulsion coating materials, E1/T1 and E2/T1, present higher reflectance than conventional tile substrate, and the curves begin to increase approximately at 350 nm. However, the application of emulsion 3 on tile (E3/T1) shows the lowest reflectance of them. In this case, the increment the UV absorbance (200–400 nm) by the TiO_2 emulsion coatings respect to the conventional tile material is noticeable.

It is also evident that the changes in reflectance data of emulsion coating on asphalt is higher than their equivalents on tiles. The different behavior evidences the influence of the substrate in the resulting reflectance values.

Conventional T2 has the higher reflectance of all the materials with a range of 0.15-0-89 a.u.from 350 nm until the end. Its functionalized equivalent (B1/T2) presents a slightly shift of the absorbance edge in the UV range, that can be attributed to the incorporation of UV-absorbent TiO_2-nanosize photocatalyst additive, but the curve is almost the same on the remaining range. T3 grows from 0.11 to 0.34 a.u.at 600 nm, and the curve stays virtually stable from that wavelength. In contrast, B2/T3 grows up at 300 nm to 0.53 a.u., which may be related with the slightly different color of these factory-supplied tiles (grey-brownness grey).

The highest distance from a 'perfect' white, WI, is as expected, the conventional dark asphalt materials. A slightly decrease on WI is observed by the application of every emulsion coating on asphalt substrate (E1/A to E3/A). The lighter ones remain to be S1/A and S2/A due to the photocatalytic coating with cementitious white/grey slurries. The values keep oscillating between similar ones on conventional and TiO_2 modified tiles with the previous emulsion coatings applications. The slightly differences seem to be assumed that are related due to in-material color variation. T2 and B1/T2 materials has the smallest whiteness index without significant differences between them. However, the factory-supplied tiles with TiO_2 built-in (B2/T3) show significant differences between their respective non-TiO_2 material (T3). As previously indicated, these factory-supplied tiles shows grey-brownness grey colour.

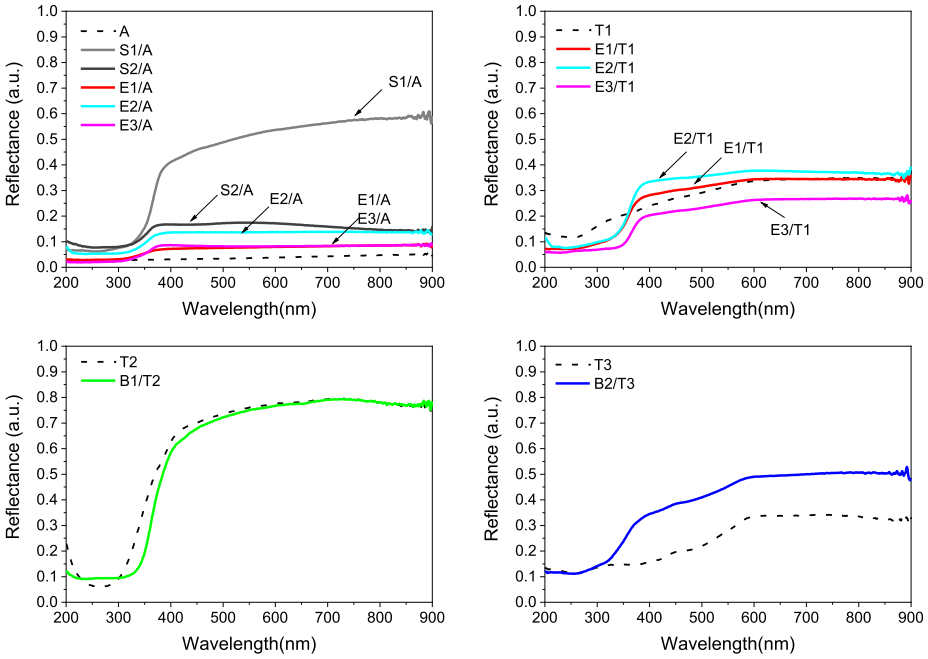

Fig. 5. Spectral reflectance of TiO_2 functionalized samples and comparison with the reference materials.

Table 2
Integrated reflectance data divided in the three main wavelength regions UV, visible and nearinfrared, and the total spectra range measurement (R_{UV}, R_{Vis}, R_{NIR} and R_T), CIELab color coordinates, whiteness index parameter (Eq.1) and the naked-eye colour of the analysed materials.

Material	$R_{UV\ (200\text{-}400\ nm)}$	$R_{Vis\ (400\text{-}700\ nm)}$	$R_{NIR\ (700\text{-}900\ nm)}$	$R_{T\ (200\text{-}900\ nm)}$	L	a	b	WI	colour
A	6	11	9	26	17.07 ± 3.78	1.03 ± 0.12	1.82 ± 0.20	82.95 ± 3.78	Black
S1/A	27	152	115	295	74.15 ± 3.44	0.80 ± 0.13	7.48 ± 0.42	26.92 ± 3.41	White
S2/A	21	51	29	101	56.64 ± 4.38	0.65 ± 0.25	4.40 ± 0.96	43.58 ± 4.43	Grey
E1/A	8	23	17	49	34.28 ± 5.56	0.85 ± 0.15	6.48 ± 1.15	66.04 ± 5.45	Black
E2/A	15	41	27	84	22.06 ± 6.56	0.47 ± 0.27	2.89 ± 1.43	77.99 ± 6.55	Black
E3/A	8	25	17	50	21.11 ± 2.95	0.61 ± 0.30	1.01 ± 1.31	78.90 ± 2.95	Black
T1	33	93	69	195	63.29 ± 0.62	1.30 ± 0.09	6.26 ± 0.30	37.27 ± 0.61	Grey
E1/T1	25	97	68	192	65.06 ± 1.26	1.11 ± 013	5.40 ± 0.37	35.37 ± 1.31	Grey
E2/T1	28	109	73	211	63.08 ± 0.28	1.06 ± 0.18	4.78 ± 0.81	37.24 ± 0.23	Grey
E3/T1	18	73	53	145	59.69 ± 0.90	1.29 ± 0.22	5.84 ± 0.63	40.75 ± 0.89	Grey
T2	45	224	155	425	89.49 ± 0.27	0.14 ± 0.01	3.92 ± 0.10	11.21 ± 0.27	White
B1/T2	36	220	155	412	89.32 ± 0.37	0.05 ± 0.04	4.04 ± 0.37	11.41 ± 0.47	White
T3	27	81	66	174	62.78 ± 1.52	5.42 ± 058	14.49 ± 0.87	40.31 ± 1.72	Grey
B2/T3	36	133	100	269	76.52 ± 0.51	2.14 ± 0.24	6.89 ± 0.38	24.56 ± 0.59	Grey

Concerning the relationship between spectral reflectance and the whiteness index (WI), Fig. 6 illustrates the linear fitting of WI and reflectance in different solar spectral regions. The regression evidences a good linear correlation between WI and the reflectance data in all solar spectral region. UV reflectance data present a good correlation with the WI. Previous results show that darker or more intense colours tend to have better UV absorption [39]. Similarly, [11], the color lightness (L* coordinate of CIELAB) is related with reflectance in visible region (400 nm–700 nm), however it does not influence the spectral reflectance in NIR light region (700 nm–2500 nm), especially in the long wave (1100 nm–2500 n m) range. These findings do not call into question the assessments set out in Fig. 5, because in our evaluation the correlation is only analysed in the short wave NIR region (700–900 nm). A linear correlation can be observed between the WI and L* using the data included in Table 2 (R^2 = 0.99) because the tested materials are in white-black scale. However, WI parameter is probably more appropriate to analyse the influence on the reflectance spectra, especially when making comparison between materials with different colour range. It implies the use of the absolute colour of samples by using the colour channels, a* and b*. The confirmation of these hypotheses is out of the scope of this paper and this is being studied next by the authors.

3.3. Surface texture

Some examples of the surface texture profiles generated from the photographs taken to the analysed materials by the digital-image processing are reproduced in Fig. 7. The 3D profiles reveal obvious differences between surfaces for the plain asphalt (A) and samples S1/A and S2/A, where slurry S2 filled the voids, generating smoother surfaces. Other examples are T2 and the equivalent with TiO_2 built-in material, B1/T2, which both shown almost smooth surface, regardless the TiO_2 incorporation. The profiles were subsequently translated into the surface roughness parameter, R*a* (pixels). The respective values are shown in Fig. 8 for all the materials studied.

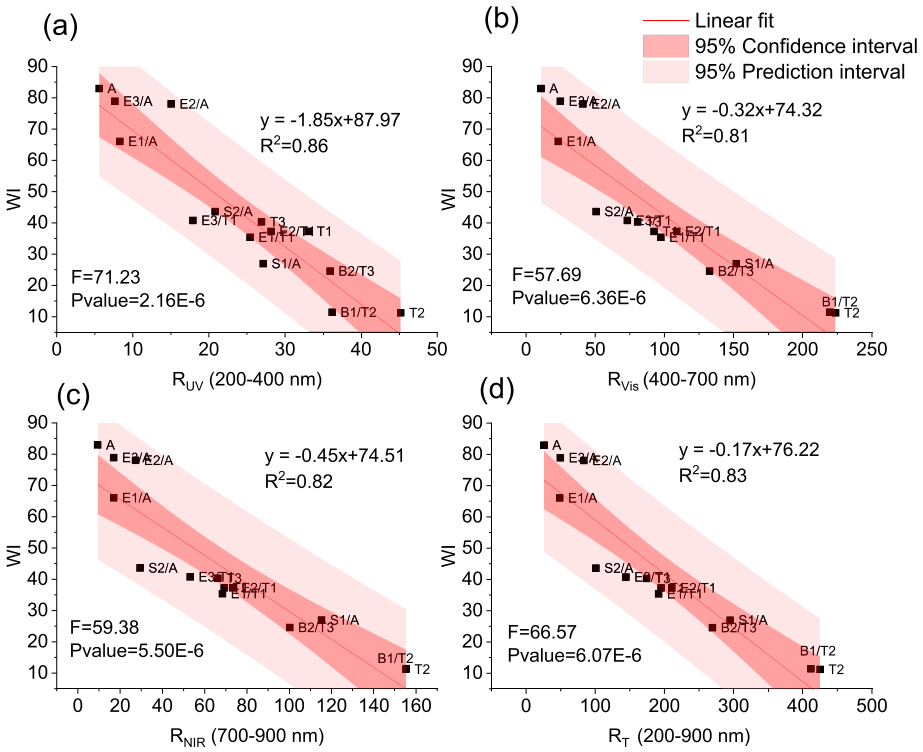

Fig. 6. Scattered plot and linear fitting result of (a) R_{UV}, (b) R_{Vis}, (c) R_{NIR}, (d) R_T and WI of the tested materials.

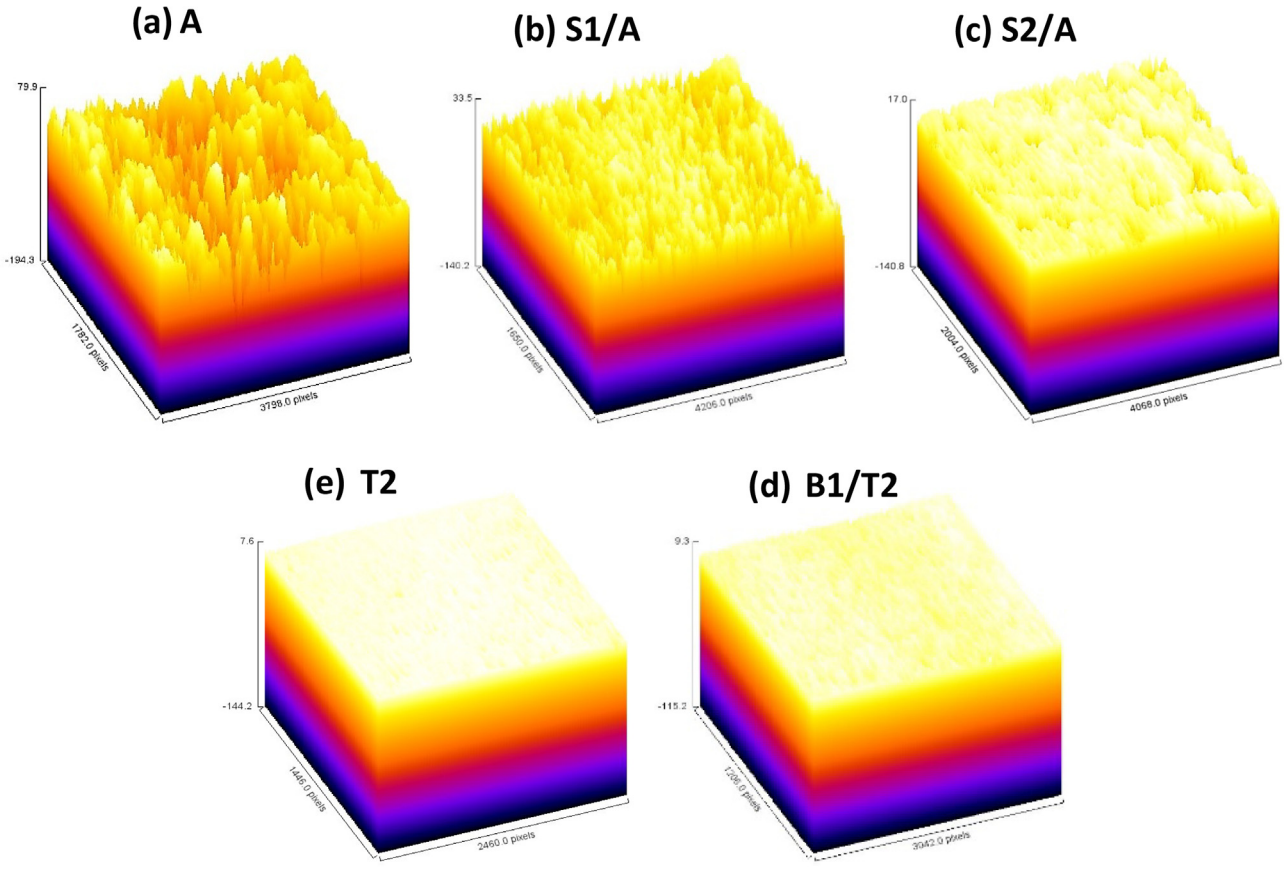

Fig. 7. Example of 3D roughness profiles for (a) conventional asphalt (A), (b-c) asphalt functionalized with TiO_2 cementitious slurry (S1/A and S2/A), (d) conventional tile (T2), and (e) tile with TiO_2 built-in (B1/T2).

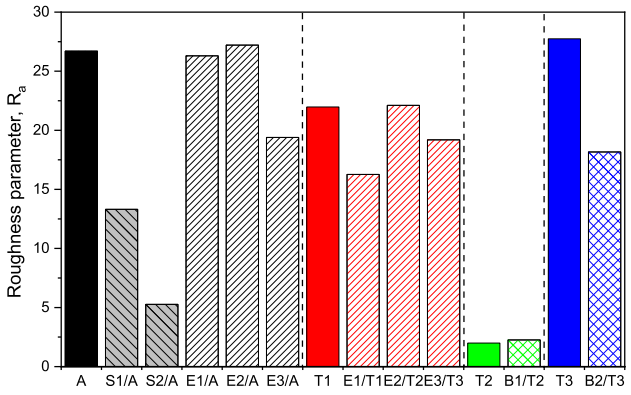

Fig. 8. Surface roughness, R_a (pixels), for all the materials studied.

3.4. Thermographic evaluation on pilot scale on outdoor exposure conditions

Table 3 include the corrective parameters (reflected apparent temperature and emissivity) needed to transform relative surface temperatures given by the thermographic technology into absolute temperatures. 'ε (IRT)' is the data obtained via infrared thermography following the ISO 18434-1:2008(E) standard. 'ε (Em.1)' and 'ε (Em.2)', are duplicate measurements performed with the emissivity-meter. Column named 'ε (TOT)' is the average of the three previous measurements, which is the data selected as a corrective parameter on the thermographic pictures.

Emissivity values do not show significant variations by the application of the nano-TiO_2 additive. Asphalt materials, remain very high (0.95 to 0.98), Tile (T1) oscillates between 0.93 and 0.96, so lower values than asphalts, but still without differences between TiO_2 nanofuncionalised and conventional material. Lowest values correspond to T2 and T3 (0.91–0.95).

Fig. 9 presents the thermographic pictures taken during a 12-hour period. Graphic temperature scales are set between −5 °C and 30 °C. The picture notes that the heat is not evenly distributed in some samples. In conventional asphalt platforms this can be due to its roughness and porous surface texture, the existence of moisture on one side of the platform or even the platform's heat transfer effects. This heat layout does not change by the emulsion coating applications (E1/A to E3/A). However, the heterogeneous distribution is accentuated in S1/A and S2/A, probably due to a non-uniform application of the TiO_2 cementitious slurry coating, therefore the existence of uneven color on the surface. On tiles, a different distribution of heat is observed, and its more clear that the heat is being retained in joints and borders of the platforms, whereas other unevenness can be also attributed to differences of color, photocatalytic coating or heating transfer [1]. Due to the non-uniformity surface temperature distribution, the treatment of IR thermography analysis has be done using the average temperature values [18].

The estimated mean hourly surface temperature values and temperature range for each material separately in function of the four substrate evaluated are given in statistical box plots (Fig. 10). The lower and upper lines of the box plots are the minimum and the maximum values of the corresponding mean hourly surface temperature values. On initial observation, it appears widespread that the mean daily surface temperature and temperature range of the TiO_2 modified materials are slightly lower than their corresponding conventional material.

The mean hourly surface temperature comparison of all materials was, in ascending order: B1/T2 < T2 < S2/A < B2/T3 < S1/A < E3/T1 < E1/T1 < E2/T1 < T1 < T3 < E2/A < E3/A < E1/A < A. Minimum values of the mean daily and the maximum surface temperatures were observed for the smooth and white coloured material tiles (B1/T2 and T2). The incorporation of a TiO_2 additive implied a slightly variation respecting the original one. On the contrary, maximum corresponding values were noticed on the rough and dark coloured material asphalts (E2/A < E3/A < E1/A < A). Application of both TiO_2 cementitious slurries onto asphalt substrate (S1/A and S2/A) induce a significant decrease of surface temperature. Both products act as a coating to be laid on the existing asphalt that cover the material cavities with a uniform layer; and imply a variation of colour to white and grey respectively. The emulsion coatings induce a lower variation of temperature respecting their corresponding substrate (asphalt, A, or tile, T1) since no fundamental changes of colour and surface roughness are involved. The factory-supplied tile with TiO_2 built-in (B2/T3) shown clearly better behaviour that their same tile without TiO_2 (T3) due to a smoother surface. Registered differences of thermal behaviour between samples will be discussed in more detail in the Sections 3.5 and 3.6.

Fig. 11a shows the surface temperature distribution for the tested materials together with the air temperature during the total experimental 12-hours period. All the platforms' surface temperature curves follow the same path. They are at its lowest temperatures (−10 to −2.5 °C) at the first hours of the day, corresponding with the lowest air temperatures of the day (3.46 °C). Then, the curve start raising until approximately 2 or 3 p.m. where its peak occurs, descending again rapidly until 4 or 5 p.m., and keeping the decrease until 8 p.m. in a more moderate

Table 3
Reflected apparent temperature (T_{refl}) and Emissivity (ε) parameters.

Material	T_{ref}(°C)	ε(IRT)[1]	ε(Em.1)[2]	ε(Em.2)[2]	ε(TOT)[3]
A	26.07 ± 2.97	0.94 ± 0.03	0.97 ± 0.01	0.94 ± 0.01	0.95 ± 0.02
S1/A	23.50 ± 0.85	0.96 ± 0.01	0.95 ± 0.07	0.97 ± 0.02	0.96 ± 0.01
S2/A	22.80 ± 0.70	0.94 ± 0.01	0.91 ± 0.04	0.95 ± 0.01	0.94 ± 0.02
E1/A	22.53 ± 0.32	0.95 ± 0.01	0.97 ± 0.01	0.98 ± 0.01	0.97 ± 0.02
E2/A	21.43 ± 0.64	0.98 ± 0.02	0.99 ± 0.01	0.98 ± 0.01	0.98 ± 0.01
E3/A	21.37 ± 0.31	0.99 ± 0.02	0.98 ± 0.01	0.98 ± 0.02	0.98 ± 0.00
T1	25.93 ± 0.55	0.93 ± 0.03	0.94 ± 0.01	0.92 ± 0.01	0.93 ± 0.01
E1/T1	22.77 ± 1.43	0.94 ± 0.01	0.94 ± 0.02	0.95 ± 0.02	0.94 ± 0.01
E2/T1	21.17 ± 0.40	0.95 ± 0.01	0.95 ± 0.01	0.98 ± 0.01	0.96 ± 0.02
E3/T1	20.60 ± 1.15	0.95 ± 0.01	0.95 ± 0.00	0.93 ± 0.01	0.94 ± 0.01
T2	23.87 ± 1.59	0.93 ± 0.02	0.87 ± 0.01	0.92 ± 0.00	0.91 ± 0.03
B/T2	22.27 ± 1.05	0.96 ± 0.01	0.88 ± 0.01	0.90 ± 0.01	0.91 ± 0.04
T3	23.87 ± 1.59	0.93 ± 0.02	0.87 ± 0.01	0.92 ± 0.00	0.91 ± 0.03
B/T3	22.00 ± 0.36	0.96 ± 0.02	0.94 ± 0.01	0.96 ± 0.01	0.95 ± 0.01

[1] data obtain via infrared thermography technology following the ISO 18434–1:2008(E) standard. [2] duplicate measurements performed with an emissivity measurement tool. [3] Average of the three previous data.

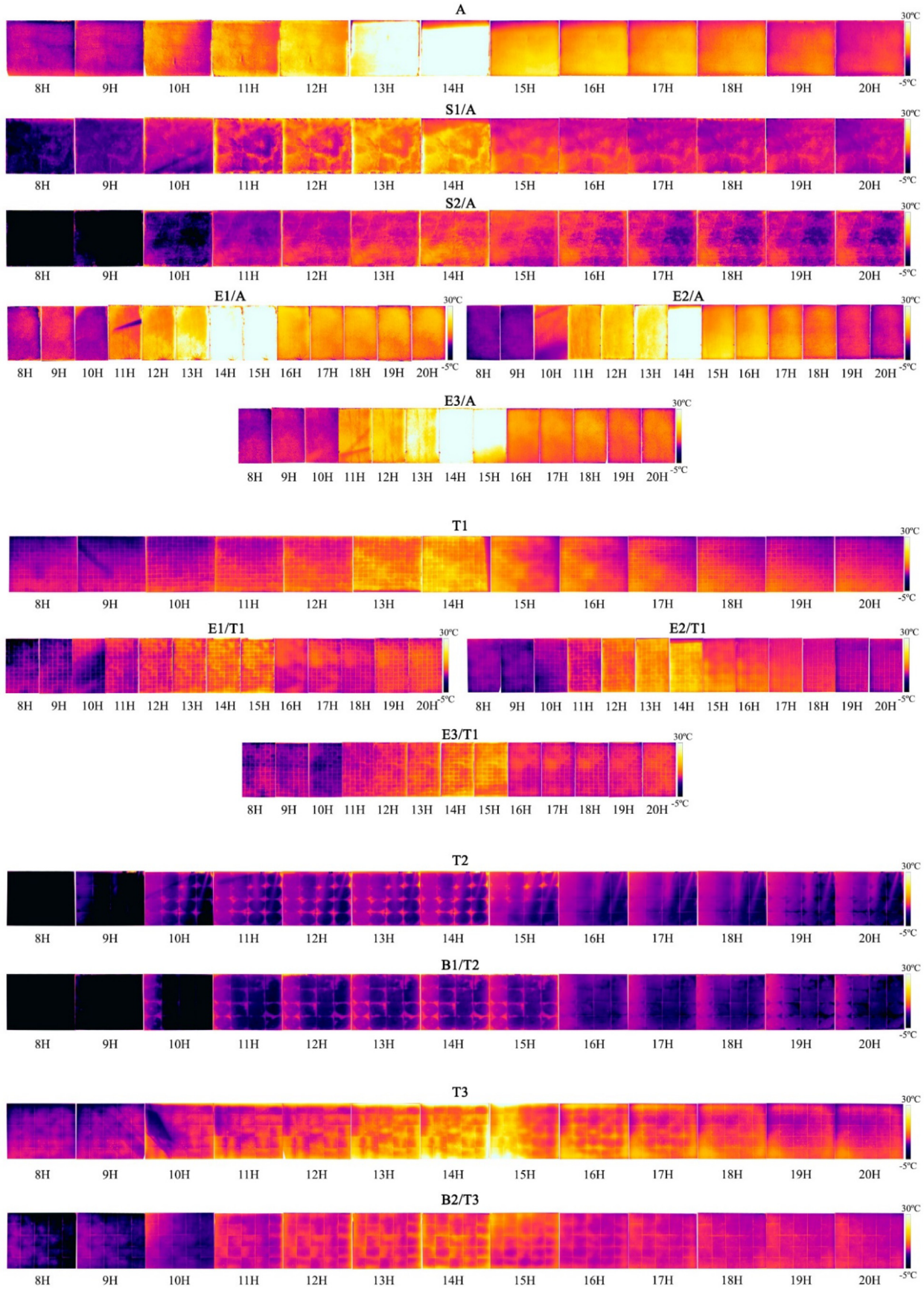

Fig. 9. Infrared images of conventional and TiO_2 functionalized materials during the 12-hour period.

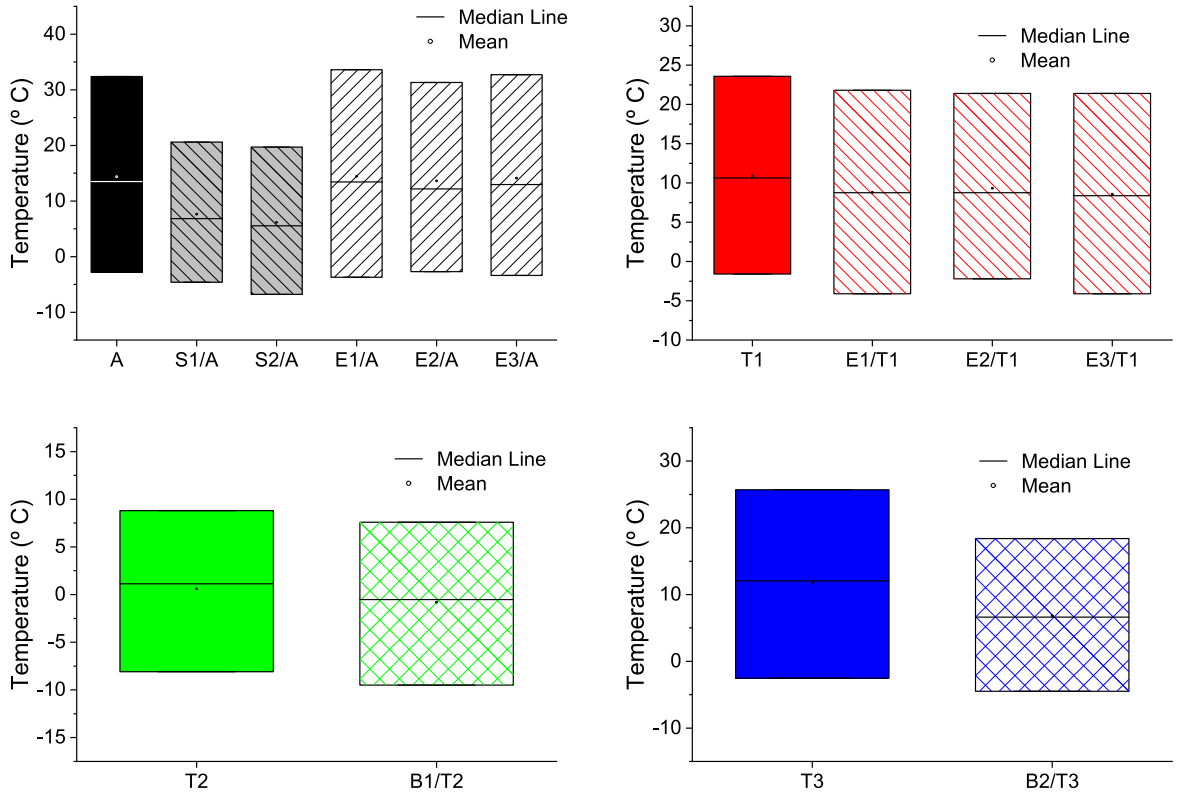

Fig. 10. Box plots of mean surface temperature within 8:00 to 20:00 for the materials studied divided in function of the substrate construction materials.

way. Whereas the air temperature peak takes place at 4 p.m. Materials S1/A and S2/A only hit the 20 °C mark at 2 p.m. meaning the cementitious slurries applications enhance the thermal behaviour of plain asphalt. Due to filled voids generating smoother surfaces, as previously explained, and imply a variation towards lighter colour (black to white or grey). Conventional and TiO_2 emulsion-coated asphalts, reached the highest surface temperature (up to 35 °C between 2 p.m. and 3 p.m), even much higher than the air temperature at that time (12–13 °C). However, it is also observed that E1/A and E3/A store heat and then release more slowly than the other ones. This conduct also repeated on tile material with the same emulsions (E1/T and E3/T1). As both emulsion applications not induce significate change of emissivity values (see Table 3), this thermal inertia effect can be attributed to those TiO_2 emulsion coatings have a lower thermal conductivity. E2/T1 varies by reaching the 20 °C at 2 p.m. and then, its surface temperature descends more rapidly than the other two. With T2 and B1/T2 a notable difference can be observed respecting the other materials, because, surface temperature of the tiles is always under the air temperature. Furthermore, the thermal inertia behaviour is also repeated on the tiles with TiO_2 built-in. Finally, a clear gap between T3 and B2/T3 is registered, where the surface temperature difference is mainly a constant of 4 °C, except at 3 p.m. when a difference of 9.4 °C is registered.

The simultaneous differences in surface temperature between the reference material and of the TiO_2 materials were depicted in Fig. 11b. As previously described, the higher decrease of surface temperatures is observed on slurry applications onto asphalt substrate (S1/A and S2/A) (down to 14.1ªC difference at 1 p.m.). E2/A also maintains lower temperatures than conventional asphalts during the whole experimental time period, with a temperature differences of 1 °C to 2ªC, except at 10 a.m. where the surface temperature difference is 4.8 °C. In contrast, E1/A and E3/A, achieve an 8 ªC temperature decrease at 10 a.m. but increase its surface temperature up to 14.4 °C at 3 p.m. regarding conventional asphalt surface temperature. This behavior is repeated on tiles samples (E1/T1 and E3/T1), displaying higher surface temperature at 3 p.m. than the non-photocatalytic one. Regarding B1/T2, it shows oscillating negative values down to −3,6 °C respecting their tile material without TiO_2, but positive 0.8 °C temperature at 15 h. Finally, about B2/T3, the surface temperature is always lower than on the non-photocatalytic one (T3) with values of −2 °C down to −9.4 °C.

3.5. Influence of the TiO_2 functionalization

Integration of the curves in Fig. 11b provides a mean quantitative value of the effect of the TiO_2 addition on the surface of the different materials. The obtained value has been correlated versus the percentage of NOx degradation (RNOx), and the WI and roughness diferrences between the photocatalytic and the corresponding twin reference material (designed as: _ref) (Fig. 12 a-c). It can be seen that a lower temperature does not seem to be related to the photocatalytic activity itself. Differences in the parameter WI give a better correlation but not good enough. Differences in roughness seem to be the most relevant parameter to induce a cooling effect.

A multiple correlation of the three variables (Fig. 12-d, Table 4) gives an acceptable correlation, finding R^2 = 0.837 between the observed and predicted values. Adjusted R^2 = 0.755, that corrects for the increase of R^2 with the number of dependent variables by taking into account the number of degrees of freedom. The parameter "statistic F" is the ratio between the regression mean square and the mean square error. The larger F the better. It is used to check the overall statistical significance of the model by means of a hypothesis test based on Fischer's F distribution. The specific objective of this test is to reject the hypothesis that all the bi parameters (associated with the variables Xi) are equal to zero.

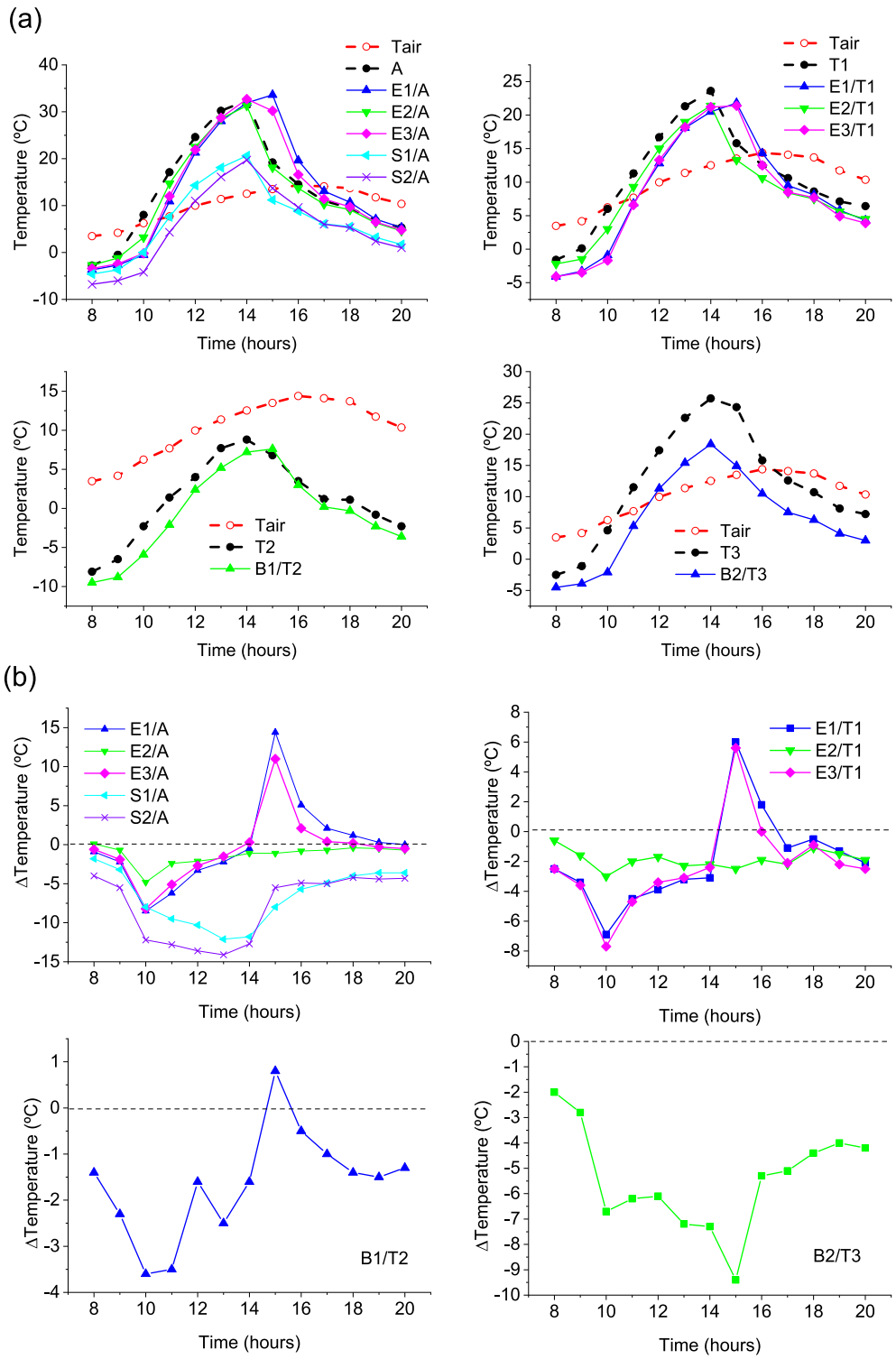

Fig. 11. (a) Distribution of mean temperature of air and surface temperatures within 8:00 to 20:00 of all tested materials and (b) instantaneous temperature differences between conventional and TiO_2 modified materials.

This hypothesis is rejected if F is greater than or equal to a limit value F*, associated with a certain objective probability of the distribution, normally p* = 0.05. The same can also be expressed by saying that the probability that F* > F must be lower than the objective probability p*. In our case, p = 0.00888 which is < 0.05, so the model, even not very good, can be accepted.

Thus, the proposed equation giving the mean diminution of the surface temperature from 8 a.m. to 8 p.m. due to TiO_2 functionalization of the material is:

$$DT(^{\circ}C) = -31.93 - 0.66RNOx(\%) + 0.5(E - WI\_ref) + 2.94(Ra - Ra\_ref)$$

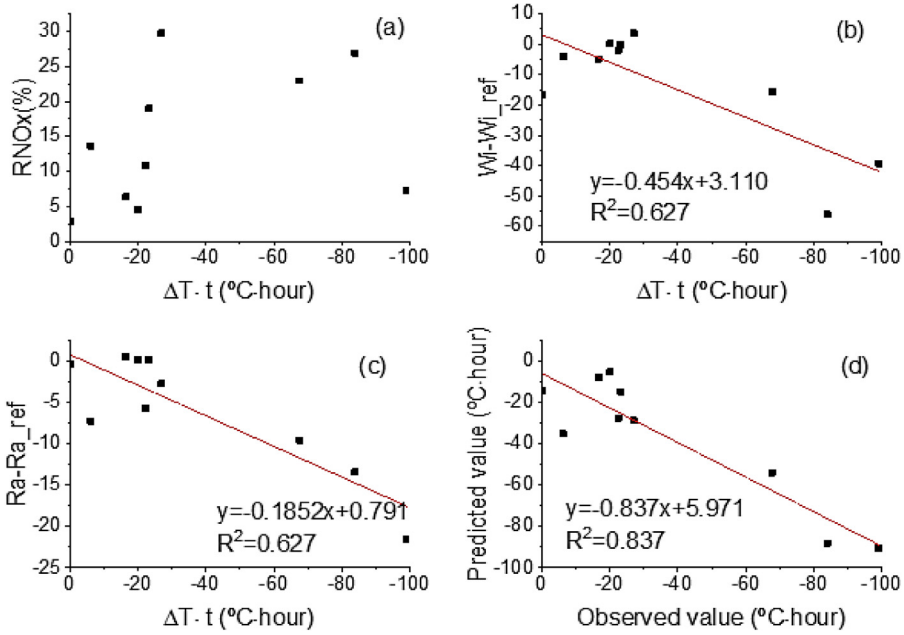

Fig. 12. Values resulting from the integration of the curves of surface temperature differences between conventional and TiO_2 modified material versus a) percentage of NOx degradation (RNOx), and b) WI and c) roughness difference between the photocatalytic and the corresponding twin reference material (denoted as _ref) (d) predicted values vs. observed values from a multiple regression analysis.

Table 4
F-ANOVA test of the differences of mean surface temperatures between TiO_2- modified and conventional materials with respect to their values of RNOx, and variation of WI and Ra parameters.

	Value	Standard error	t-value	Prob > [t]	Number of points	10
Intercept	−2.6609	10.4340	−0.2550	0.8072	Degrees of freedom	6
RNOx	−0.6642	0.5900	−1.1259	0.3032	Residual sum of Square	1708
Wi-Wi_ref	0.50290	0.4660	1.1275	0.3026	R Square (COD)	0.840
Ra-Ra_ref	2.9400	1.2153	2.4169	0.0521	Adj. R Square	0.755
Anova	DF	Sum of Square	Mean Square	Fvalue	Prob > F	
Model	3	8769	2923	10.267	0.0089*	
Error	6	1708	284.7	–	–	
Total	9	10,477	–	–	–	

*at the 0.05 level, the population means significantly different

Concerning t-statistics, ratios between the forecast and its standard deviation, generally a t > 2 value is acceptable. In our case, it is only true for the variable Ra-Ra_ref, as it also reflects the corresponding p-value (p = 0.052), which is the only one below the objective probability of 0.1, which is usually used for this test. The others exceed this threshold, so these variables do not contribute significantly to the explanation of the variance of the independent variable. Thus, the lower temperature in the photocatalytic samples can be attributed to the smoother surface due to the addition of the photocatalyst.

3.6. Influence of reflectance, color and texture surface properties on the thermal behavior of materials

To investigate the impact of solar reflectance, colour and surface texture on surface temperatures, the correlation with the previous parameters: total solar reflectance (Rt), the whiteness index (WI) and roughness (Ra) parameters was explored (Fig. 13). The regression results evidence that all parameters show a linear correlation with temperature. For each relationship exhibited the simplest model (linear trend) with R^2 that has range from 0.72 to 0.84, being the more dominant factor the surface roughness. In the premise of 95% confidence interval, the ANOVA test was conducted and P values demonstrates that the regression equations pass the test and the fitting results are reliable (data included inside the Fig. 13).

These results are in accordance with previous published works [11,18,40,41]. Xie et. al. [11] stablished that the reflectance between 400 nm and 1100 nm is a significant factor to influence the thermal performance of reflective coatings. The long wave near-infrared light region could be excluded in reflectance optimal design when considering the cooling effect. In [11,18] it was found that in general, the smooth surfaced materials present lower surface temperatures than the ones with rough surface and the light colored tiles were cooler than the others.

Data was analysed by one-way ANOVA method with 95% confidence interval and Bonferroni Test, Tables 5 and 6 respectively, to check the reliability to differ samples in terms of colour and roughness divided the collected data into different groups. Three colour categories were used according to the naked-eye colour (white, grey and black, see Table 2). The surface roughness was divided also in three categories basis on the Ra parameter: smooth (≤20), mean (>20–30) and rough (≥30). Differences of the mean surface temperatures of the studied materials with three different colours were found statistically significant at the confidence level of 0.05. In contrast, the mean surface temperature is not statistical different on mean and rough samples, although is significant with the smooth surface. As a result, both colour and surface roughness

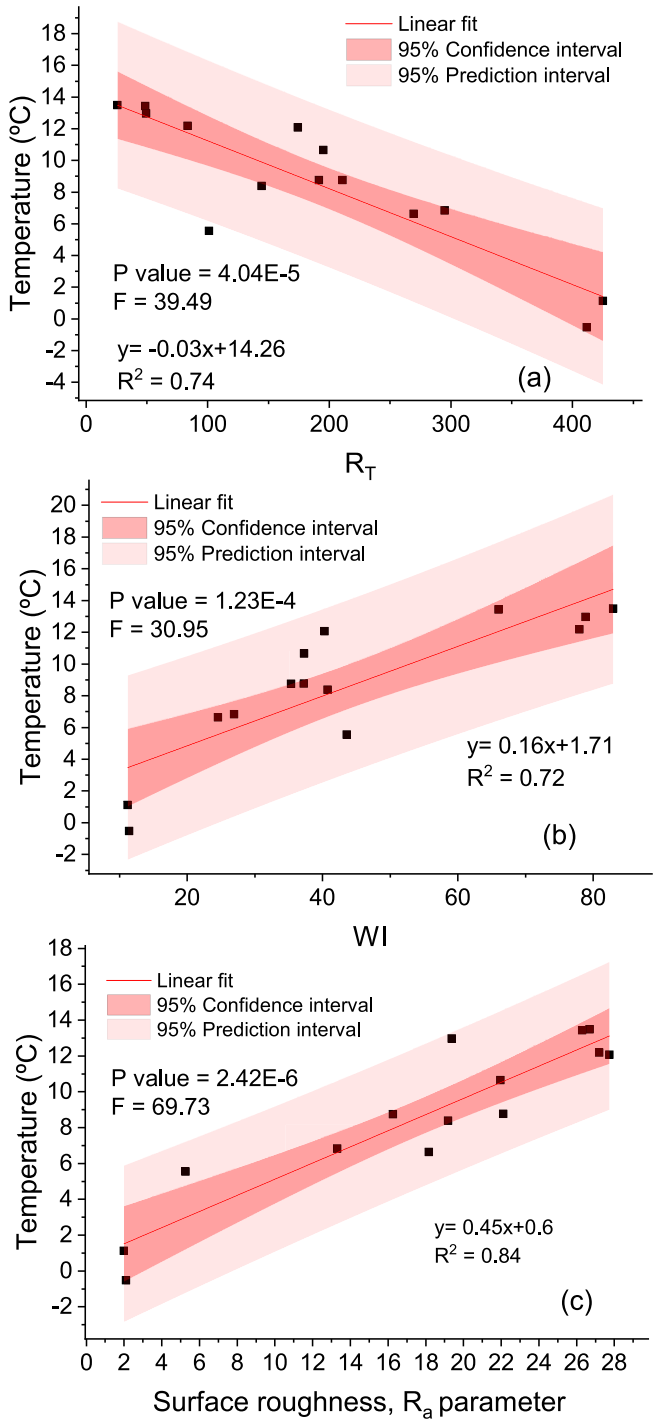

Fig. 13. Scattered plot and linear fitting result of (a) total solar reflectance (R_T), (b) Whiteness index (WI), (c) Surface roughness (Ra) and mean surface temperature of the tested materials.

are crucial parameters that should be taken into account for pavement engineering to contribute to the mitigation of the urban heat island effect.

The TiO_2 application type (emulsion, slurry and built-in) and the substrate construction material were also evaluated using the same statistical analysis. Results evidence that both are not influencing the surface temperature (data not included). This is due to that this statistical analysis encompasses all materials with different textures and colours, therefore the significance of both factors prevails over other parameters. In fact, in general, asphalt experiment higher temperatures respect to the tiles materials. A comparison only of the TiO_2 emulsion coating materials, since no fundamental changes of colour and surface roughness of substrates are involved, demonstrated the significant influence of the substrate (asphalt or tile) in the resulting thermal behaviour (Fvalue = 42.52 and Prob > F = 6.29 E^{-4}).

Table 5
F-ANOVA test of mean surface temperatures of materials with respect to their colour and roughness divided into three categories.

	R Square	DF	Quadratic Sum	Mean Square	Fvalue	Prob > F
Colour (white, grey and black)						
Model	0.76	2	190.54	95.27	17.35	3.96E−4*
Error	–	11	60.39	5.49	–	–
Total	–	13	250.93	–	–	–
Roughness (smooth, mean and rough)						
Model	0.75	2	188.87	94.44	16.74	4.6E−4*
Error	–	11	62.06	5.64	–	–
Total	–	13	250.93	–	–	–

*at the 0.05 level, the population means significantly different

Table 6
Bonferroni test of mean surface temperatures of materials with respect to their colour and roughness divided into three categories.

	Mean difference	Std. error	t value	Prob	Sig.*	LPC	UPC
Colour							
White-Black	−10.54	1.79	−5.89	3.12E−4	1	−15.59	−5.49
Grey-Black	−4.33	1.47	−2.95	0.040	1	−8.47	−0.19
Grey-White	6.21	1.62	3.84	0.008	1	1.65	10.77
Roughness							
Mean – Rough	−3.05	1.44	−2.12	0.17	0	−7.11	1–00
Smooth- Rough	−9.71	1.68	−5.79	3.66E−4	1	−14.45	−4.98
Smooth- Mean	−6.67	1.73	−3.84	0.008	1	−11.55	−1.77

*1 and 0 indicate that the difference of the means is significant and not significant at the 0.05 level respectively; LPC lower control limits; UPC upper control limits.

4. Conclusions

10 TiO_2 based photocatalytic pavement were evaluated versus their corresponding reference non photocatalytic materials (conventional asphalt and tiles substrates) for their thermal properties in outdoor conditions. The materials' thermal balance is determined mainly by their reflectivity to solar radiation and their emissivity to the long wave radiation. As the emissivity values do not show significant variations by the application of the nano-TiO_2 additives, the improved thermal behavior of all these functionalized materials compared to the conventional ones can be due to the different physical modifications that imply those treatments in their reflective behaviour. These changes are essentially due to the colour and surface texture (roughness). In general, TiO_2 treatments lead to smoother and lighter-coloured surfaces that tend to absorb less solar radiation, having found, in all the cases, lower mean daily surface temperatures. A multiple correlation including photocatalytic efficiency, and differences in whitening index and texture gives an acceptable correlation, finding R^2 = 0.837 between the observed and predicted values. The statistical model indicates that the main contribution to the lower temperature in the photocatalytic samples is due to the smoother surface due to the addition of the photocatalyst.

5. Formatting of funding sources:

The authors would like to thank the financial support provided by LIFE program's (LIFE PHOTOSCALING-LIFE13 ENV/ES/001221),

national project (BIA2016-79582-R, TEVALRISK) and from Fundación General del CSIC (Programa ComFuturo) for the research contract of Eva Jimenez-Relinque. Also acknowledge the introduction to research Scholarship JAE-Intro (October 2019 - June 2020) in the ISCMA (Sustainable Interaction between Construction Materials and the environment) research group of IETcc (Construction Science Institute Eduardo Torroja) belonging to the CSIC (Spanish National Research Council).

Declaration of Competing Interest

The authors declare that they have no known competing financial interests or personal relationships that could have appeared to influence the work reported in this paper.

References

[1] E. Carnielo, and M. Zinzi, Optical and thermal characterisation of cool asphalts to mitigate urban temperatures and building cooling demand. Building and Environment, 2013. 60: p. 56-65 %@ 0360-1323.
[2] N.L. Alchapar, E.N. Correa, M.A.J.A.c. Cantón, Índice de reflectancia solar de revestimientos verticales: potencial para la mitigación de la isla de calor urbana. 2012. 12(3): p. 107-123.
[3] C. Alonso et al., Effect of façade surface finish on building energy rehabilitation. Solar Energy, 2017. 146: p. 470-483 %@ 0038-092X.
[4] Correa, É.N., S. Flores Larsen, and G.J.A.e.E.R.y.M.A. Lesino, Isla de calor urbana: Efecto de los pavimentos. Informe de avance. 2003. 7.
[5] S. Hassid et al., The effect of the Athens heat island on air conditioning load. 2000. 32(2): p. 131-141.
[6] M. Santamouris et al. On the impact of urban climate on the energy consumption of buildings. 2001. 70(3): p. 201-216.
[7] Papadopoulos, A.M.J.E. and Buildings, The influence of street canyons on the cooling loads of buildings and the performance of air conditioning systems. 2001. 33(6): p. 601-607.
[8] M. Kolokotroni et al., Heating and cooling degree day prediction within the London urban heat island area. 2009. 30(3): p. 183-202.
[9] T. Ihara et al., City-block-scale sensitivity of electricity consumption to air temperature and air humidity in business districts of Tokyo, Japan. 2008. 33 (11): p. 1634-1645.
[10] J.M.C. Prats, S.M. Vicente-Serrano, and M.A.S.J.B. Sánchez, Los efectos de la urbanización en el clima de Zaragoza (España): La isla de calor y sus factores condicionantes. 2005(40).
[11] N. Xie et al., Laboratorial investigation on optical and thermal properties of cool pavement nano-coatings for urban heat island mitigation. Building and Environment, 2019. 147: p. 231-240 %@ 0360-1323.
[12] L.S. Rose, H. Akbari, and H. Taha, Characterizing the fabric of the urban environment: a case study of Greater Houston, Texas. 2003, Lawrence Berkeley National Lab.(LBNL), Berkeley, CA (United States).
[13] M. Santamouris, Using cool pavements as a mitigation strategy to fight urban heat island—a review of the actual developments, Renew. Sustain. Energy Rev. 26 (2013) 224–240, %@ 1364-0321.
[14] M. Santamouris, A. Synnefa, T. Karlessi, Using advanced cool materials in the urban built environment to mitigate heat islands and improve thermal comfort conditions, Solar Energy 85 (12) (2011) 3085–3102, %@ 0038-092X.
[15] A. Mohajerani, J. Bakaric, T. Jeffrey-Bailey, The urban heat island effect, its causes, and mitigation, with reference to the thermal properties of asphalt concrete, J. Environ. Manage. 197 (2017) 522–538, %@ 0301-4797.
[16] Y. Qin, A review on the development of cool pavements to mitigate urban heat island effect. Renewable and sustainable energy reviews, 2015. 52: p. 445-459 %@ 1364-0321.
[17] A. Synnefa, M. Santamouris, K. Apostolakis, On the development, optical properties and thermal performance of cool colored coatings for the urban environment, Solar Energy 81 (4) (2007) 488–497.
[18] L. Doulos, M. Santamouris, I. Livada, Passive cooling of outdoor urban spaces. The role of materials, Solar Energy 77 (2) (2004) 231–249, %@ 0038-092X.
[19] M. Santamouris et al., Using cool paving materials to improve microclimate of urban areas–Design realization and results of the flisvos project. Building and Environment, 2012. 53: p. 128-136 %@ 0360-1323.
[20] G.E. Kyriakodis, M. Santamouris, Using reflective pavements to mitigate urban heat island in warm climates-Results from a large scale urban mitigation project. Urban Climate, 2018. 24: p. 326-339 %@ 2212-0955.
[21] L.-w. Shen et al., Effect of TiO 2 pigment gradation on the properties of thermal insulation coatings. International Journal of Minerals, Metallurgy, and Materials, 2016. 23(12): p. 1466-1474 %@ 1674-4799.
[22] J. Song et al., The effects of particle size distribution on the optical properties of titanium dioxide rutile pigments and their applications in cool non-white coatings, Solar Energy Mater. Solar Cells 130 (2014) 42–50.
[23] X. Tang et al., Self-cleaning and de-pollution efficacies of photocatalytic architectural membranes. Applied Catalysis B: Environmental, 2020: p. 119260 %@ 0926-3373.
[24] M. Baudys et al., Weathering tests of photocatalytic facade paints containing ZnO and TiO2. Chemical Engineering Journal, 2015. 261: p. 83-87 %@ 1385-8947.
[25] T. Maggos et al., Photocatalytic degradation of NOx in a pilot street canyon configuration using TiO 2-mortar panels. Environmental monitoring and assessment, 2008. 136(1-3): p. 35-44 %@ 0167-6369.
[26] E. Jiménez-Relinque et al., In situ evaluation of the NO x removal efficiency of photocatalytic pavements: statistical analysis of the relevance of exposure time and environmental variables. Environmental Science and Pollution Research, 2019. 26(36): p. 36088-36095 %@ 0944-1344.
[27] J.M. Cordero et al., NOx removal efficiency of urban photocatalytic pavements at pilot scale. Science of The Total Environment, 2020: p. 137459 %@ 0048-9697.
[28] E. Jimenez-Relinque et al., Characteristics and efficiency of photocatalytic cementitious materials: Type of binder, roughness and microstructure. Cement and Concrete Research, 2015. 71: p. 124-131 %@ 0008-8846.
[29] A. Laplaza et al., Photocatalytic behavior of colored mortars containing TiO2 and iron oxide based pigments. Construction and Building Materials, 2017. 144: p. 300-310 %@ 0950-0618.
[30] N. Xie et al., Optical and durability performance of near-infrared reflective coatings for cool pavement: Laboratorial investigation, Build. Environ. 163 (2019) 106334.
[31] Y. Qi, B. Xiang, and J. Zhang, Effect of titanium dioxide (TiO2) with different crystal forms and surface modifications on cooling property and surface wettability of cool roofing materials. Solar Energy Materials and Solar Cells, 2017. 172: p. 34-43 %@ 0927-0248.
[32] E. Jimenez-Relinque et al., A new holistic conceptual framework for assessment of photocatalytic pavements performance, Front. Chem. 8 (2020) 743.
[33] J. Cordero et al., NOx removal efficiency of urban photocatalytic pavements at pilot scale, Sci. Total Environ. (2020) 137459.
[34] E. Jiménez-Relinque et al., In situ evaluation of the NO x removal efficiency of photocatalytic pavements: statistical analysis of the relevance of exposure time and environmental variables, J. Environ. Sci. Pollut. Res. (2019) 1–8.
[35] E. Jimenez-Relinque et al., Characteristics and efficiency of photocatalytic cementitious materials: type of binder, roughness and microstructure, Cem. Concr. Res. 71 (2015) 124–131.
[36] M.R. Cox, M. Budhu, A practical approach to grain shape quantification, Eng. Geol. 96 (1–2) (2008) 1–16.
[37] G. Chinga et al., Quantification of the 3D microstructure of SC surfaces, J. Microsc. 227 (3) (2007) 254–265.
[38] (ISO), I.S.O., ISO 18434-1:2008 Condition monitoring and diagnostics of machines. Thermography. Part 1: General procedures. 2008. p. 24.
[39] A. Riva et al., Modeling the effects of color on the UV protection provided by cotton woven fabrics dyed with azo dyestuffs. Industrial & engineering chemistry research, 2009. 48(22): p. 9817-9822 %@ 0888-5885.
[40] J.J. Stempihar et al., Porous asphalt pavement temperature effects for urban heat island analysis. Transportation research record, 2012. 2293(1): p. 123-130 %@ 0361-1981.
[41] A. Synnefa, M. Santamouris, and I. Livada, A study of the thermal performance of reflective coatings for the urban environment. Solar Energy, 2006. 80(8): p. 968-981 %@ 0038-092X.